Comparative Evaluation of Methodologies for T-Wave Alternans Mapping in Electrograms

Michele Orini*, Ben Hanson, Violeta Monasterio, Juan Pablo Martínez, Martin Hayward, Peter Taggart, and Pier Lambiase

***Abstract*—Electrograms (EGM) recorded from the surface of the myocardium are becoming more and more accessible. T-wave alternans (TWA) is associated with increased vulnerability to ventricular tachycardia/fibrillation and it occurs before the onset of ventricular arrhythmias. Thus, accurate methodologies for time-varying alternans estimation/detection in EGM are needed. In this paper, we perform a simulation study based on epicardial EGM recorded *in vivo* in humans to compare the accuracy of four methodologies: the spectral method (SM), modified moving average method, laplacian likelihood ratio method (LLR), and a novel method based on time-frequency distributions. A variety of effects are considered, which include the presence of wide band noise, respiration, and impulse artifacts. We found that 1) EGM-TWA can be detected accurately when the standard deviation of wide-band noise is equal or smaller than ten times the magnitude of EGM-TWA. 2) Respiration can be critical for EGM-TWA analysis, even at typical respiratory rates. 3) Impulse noise strongly reduces the accuracy of all methods, except LLR. 4) If depolarization time is used as a fiducial point, the localization of the T-wave is not critical for the accuracy of EGM-TWA detection. 5) According to this study, all methodologies provided accurate EGM-TWA detection/quantification in ideal conditions, while LLR was the most robust, providing better detection-rates in noisy conditions. Application on epicardial mapping of the *in vivo* human heart shows that EGM-TWA has heterogeneous spatio-temporal distribution.**

***Index Terms*—Electrograms (EGM), intracardiac ECG, repolarization, T-wave alternans, ventricular arrhythmia.**

I. Introduction

A repeating ABAB pattern in the morphology of the ST-segment or T-wave in the ECG, so called T-wave alternans (ECG-TWA), is a phenomenon associated with arrhythmogenesis. Many studies have demonstrated the existence of a link between ECG-TWA and the risk for sudden cardiac death [1]–[4], suggesting that ECG-TWA may be used as a diagnostic and prognostic tool. Advances in the aetiology and diagnosis of ECG-TWA were partially due to the development of methodologies for the estimation and detection of ECG-TWA [5]. ECG-TWA is caused by alternation in the duration and morphology of the transmembrane potential of myocytes, a phenomenon called repolarization alternans, whose origin is currently under investigation [3], [6]. Unipolar electrograms (EGM) recorded on the surface of the myocardium offer the opportunity to study the electrical activity of the heart at the tissue level. They incorporate features from the transmembrane potential providing indirect estimates of local depolarization and repolarization times [7], and also the ECG, exhibiting a similar waveform which includes a T-wave. Several studies have demonstrated that EGM-TWA is also associated with increased vulnerability to ventricular tachycardia/fibrillation in humans, dog, and swine [8]–[11]. In particular, recent work has shown that EGM-TWA increases before the onset of ventricular arrhythmias in humans [11], [12]. This suggests that EGM-TWA may be useful as a warning of imminent ventricular tachycardia/fibrillation in implantable cardioverter defibrillator patients [12], and calls for an effort to provide the medical community with accurate and robust methodologies for the measurement of EGM-TWA. Importantly, the analysis of EGM offers the unique opportunity of studying the spatial distribution of alternans [13], [14], and in particular discordant alternans, which is a precursor to ventricular tachycardia [4]. Thus, accurate techniques for EGM-TWA assessment are needed to achieve better diagnostic reliability, and to improve the understanding of the link between repolarization alternans at the cellular level and increased risk of sudden cardiac death. However, in only few methodological studies has the accuracy of EGM-TWA estimation/detection been assessed [11], [15]. In most of the clinical studies on EGM-TWA, the same techniques used in ECG-TWA analysis are adopted, namely, the spectral method (SM) [8], [10], [13]–[15], and the modified moving average method (MMA) [16]. To the best of our knowledge, no study has assessed and compared the accuracy of these techniques in the analysis of unipolar EGM.

The purpose of this paper is to assess and compare the accuracy of four techniques for the estimation and statistical

Manuscript received June 22, 2013; revised September 22, 2013; accepted October 23, 2013. Date of publication November 6, 2013; date of current version January 16, 2014. This work was supported in part by the Medical Research Council grant (Ref G0901819), by the Department of Health's NIHR biomedical research centers funding scheme, in part by the Ministerio de Economia y Competitividad, FEDER under Project TEC2010-21703-C03-02, CIBER-BBN through Instituto de Salud Carlos III and Grupo Consolidado GTC from DGA, and in part by the European Social Fund. *Asterisk indicates corresponding author.*

*M. Orini is with the Heart Hospital, Institute of Cardiovascular Science, University College London, London WC1E 6BT, U.K. (e-mail: m.orini@ucl.ac.uk).

B. Hanson is with the Department of Mechanical Engineering, University College London, London WC1E 6BT, U.K. (e-mail: b.hanson@ucl.ac.uk).

V. Monasterio and J. P. Martínez are with the The Communication Technologies Group, Aragón Institute of Engineering Research (I3A), Universidad de Zaragoza, 50004 Zaragoza, Spain, and also with the The Biomedical Research Networking center in Bioengineering, Biomaterials and Nanomedicine, 50018 Zaragoza, Aragon, Spain (e-mail: violeta@unizar.es; jpmart@unizar.es).

M. Hayward, P. Taggart, and P. Lambiase are with the Heart Hospital, Institute of Cardiovascular Science, University College London, London WC1E 6BT, U.K. (e-mail: martin.hayward@uclh.nhs.uk; peter.taggart@uclh.nhs.uk; pier.lambiase@uclh.nhs.uk).

Color versions of one or more of the figures in this paper are available online at http://ieeexplore.ieee.org.

Digital Object Identifier 10.1109/TBME.2013.2289304

detection of EGM-TWA by means of simulations which reproduce the conditions of most electrophysiological studies. EGM-TWA was added to 120 EGM recorded from the entire epicardium in a patient undergoing cardiac surgery. Different effects are studied, which include 1) Wide-band noise, which models electrical and muscular interference; 2) respiration, which has been recognized as a possible confounding factor [17], [18] but whose effect over EGM-TWA has, to our knowledge, not been assessed; 3) impulse noise, such as loss of capture, ectopic beats, or movement artifacts; 4) The morphology of the EGM, i.e., the polarity of the T-wave and the effect of cycle length; 5) Accuracy in the temporal localization of the T-waves. Finally, application on real data demonstrates the possibility of determining the spatial distribution of EGM-TWA *in vivo* in human.

II. Methods for EGM-TWA Analysis

In this section, we describe four methodologies to estimate EGM-TWA amplitude and a statistical testing based on surrogate data analysis [19]. Estimates used for quantification are denoted as $V[b]$, while statistics used for detection are denoted as $Z[b]$, where b indicates the heart beat.

A. EGM-TWA Quantification

Three of the methods described here (SM, MMA, and LLR, see next sections for details) are used in ECG-TWA analysis and have already been described elsewhere [5]. In this study, we have slightly modified the original methods to adjust the analysis to the time-varying study of unipolar EGM, unify the detection scheme, and compare the results.

The first step is the reorganization of the data. Let $y[n]$ be the EGM low-pass filtered at 25 Hz. Activation times, $\tau[b]$, are estimated as the minimum of the first derivative during depolarization phase, in a 180 ms long window starting at the instant of stimulation, which is assumed to be known. The filtered signal is reorganized in a matrix $Y[n,b]$ of size $[N \times B]$, B being the number of beats and $N = 200$ ms the portion of the T-wave being analyzed. Each column of $Y[n,b]$, is a T-wave, evaluated at $n \in [\tau[b]+101, \tau[b]+300]$ms. A detrending filter is used to enhance changes in the T-wave morphology on a beat-to-beat basis:

$$Y_{\mathrm{D}}[n,b] = Y[n,b+1] - Y[n,b] \tag{1}$$

1) Spectral Method: The SM is probably the most commonly used in research and is also implemented in commercial equipment for ECG-TWA analysis. It uses spectral analysis to quantify the magnitude of the alternation in the morphology of the T-wave which appears every 2 beats, i.e., at a frequency equal to 0.5 cycles per beat (cpb) [5]. The aggregate spectrum, $P[b,f]$, is computed by estimating the spectrum along rows, in a moving window of length $L = 32$ centered on beat b, and averaging along n:

$$P[b,f] = \frac{1}{LN}\sum_{n=1}^{N}\left|\sum_{l=-L/2+1}^{L/2} Y_{\mathrm{D}}[n,b+l]e^{-2\pi i l}\right|^2 \tag{2}$$

where f is discrete frequency in cpb. The detection statistic is

$$Z_{\mathrm{SM}}[b] = \frac{P[b,f=0.5] - P_{\mathcal{N}}[b]}{\sigma_{\mathcal{N}}^{(\mathrm{P})}[b]} \tag{3}$$

where $P_{\mathcal{N}}[b]$ and $\sigma_{\mathcal{N}}^{(\mathrm{P})}[b]$ are the mean and standard deviation of the power content in noise band, defined for $f \in [0.44, 0.49]$cpb [5], [15]. EGM-TWA magnitude is estimated as $V_{\mathrm{SM}}[b] = \sqrt{P[b,f=0.5] - P_{\mathcal{N}}[b]}$.

2) Modified Moving Average Method: This method, which is also implemented in commercial equipment, performs nonlinear processing of $Y[n,b]$ in the time domain [5]. $Y[n,b]$ is divided into two matrices, $Y_{\mathrm{O}}[n,2b-1]$ and $Y_{\mathrm{E}}[n,2b]$. A new matrix is computed recursively as

$$\overline{Y}_{\mathrm{E}}[n,2b] = \overline{Y}_{\mathrm{E}}[n,2(b-1)] + \Delta_{\mathrm{E}}[n,2b] \tag{4}$$

where

$$\Delta_{\mathrm{E}}[n,2b] = \frac{1}{8}(Y_{\mathrm{E}}[n,2(b-1)] - \overline{Y}_{\mathrm{E}}[n,2(b-1)]). \tag{5}$$

In the original version of the method [16], the effect of outliers is reduced by limiting $\Delta_{\mathrm{E}}[n,2b]$ to a constant value. With the same purpose, in this study $\Delta_{\mathrm{E}}[n,2b]$ is bounded to $\pm\Delta_{\mathrm{E}}^{\mathrm{M}}[n]$, which is equal to the 75th percentile of $|Y_{\mathrm{D}}[n,b]|$, estimated along beats. Matrix $\overline{Y}_{\mathrm{O}}[n,2b-1]$ is estimated as in (4)–(5) using odd beats. In (4), matrices $\overline{Y}_{\mathrm{E}}[n,2b]$ and $\overline{Y}_{\mathrm{O}}[n,2b-1]$ are initialized as one eighth of the median T-wave estimated in the first eight even and odd beats, respectively. An estimate of EGM-TWA magnitude, $V_{\mathrm{MMA}}[2b]$, is obtained as the mean of $\overline{Y}_{\mathrm{O}} - \overline{Y}_{\mathrm{E}}$, while the statistic used for EGM-TWA detection is

$$Z_{\mathrm{MMA}}[2b] = \max\left|\overline{Y}_{\mathrm{O}}[n,2b-1] - \overline{Y}_{\mathrm{E}}[n,2b]\right|. \tag{6}$$

Note that the original version of the method does not include a statistical procedure for alternans detection.

3) Laplacian Likelihood Ratio Method: This method is based on median filtering and has been shown to be accurate and robust for the analysis of ECG-TWA, even when used in time-varying analysis [5], [20]. This method assumes that at each heart beat, a T-wave is the sum of an invariant T-wave, an alternans wave with alternating polarity, and Laplacian noise [20]. It can be shown that for this model, the maximum likelihood estimation of the alternans wave, computed in a moving window of length $L = 32$ and centered on beat b, is

$$v[n,b] = \mathrm{median}(\{Y_{\mathrm{D}}[n,b+l](-1)^l\}_{l=-L/2+1}^{L/2}) \tag{7}$$

and the magnitude of EGM-TWA is

$$V_{\mathrm{LLR}}[b] = 2\sqrt{\frac{1}{N}\sum_{n=1}^{N} v[n,b]^2}. \tag{8}$$

The detection statistic is the generalized likelihood test associated with the model [20]:

$$Z_{\mathrm{LLR}}[b] = \frac{\sqrt{2}}{\sigma_L[b]NL}\sum_{n=1}^{N}\left[\sum_{l=-L/2+1}^{L/2}|Y_{\mathrm{D}}[n,b+l](-1)^l \cdot M[n,l]|\right]. \tag{9}$$

In (9), $\sigma_L[b]$ is the noise level estimate:

$$\sigma_L[b] = \frac{\sqrt{2}}{NL}\sum_{n=1}^{N}\sum_{l=-L/2+1}^{L/2}|Y_{\mathrm{D}}[n,b+l] - v[n,b](-1)^l| \tag{10}$$

and $M[n,l]$ is a matrix of size $[N \times L]$ in which all elements equal zero, except those $[n,l]$ for which $\min(0, v[n,b+l]) < Y_{\mathrm{D}}[n,b+l](-1)^l < \max(0, v[n,b+l])$, for which $M[n,l] = 1$. Using $M[n,l]$ the summation in (9) is proportional to the absolute sum of the terms in the demodulated series $|Y_{\mathrm{D}}[n,b+l](-1)^l|_{l=L/2+1}^{L/2}$, whose values lie in $[0, v[n,b+l]]$ for $v[n,b+l] > 0$, and in $[v[n,b+l], 0]$ for $v[n,b+l] < 0$ [20].

4) Time-Frequency Distribution: This method is similar to the SM, but it uses continuous time-frequency analysis instead of spectral analysis. The rationale for proposing this new method is that a better time-frequency resolution than that of spectral analysis applied in moving windows may improve the detection of EGM-TWA. First, the matrix $Y_{\mathrm{D}}[n,b']$ is computed by up-sampling rows of $Y_{\mathrm{D}}[n,b]$ with an up-sampling factor equal to 2 to prevent border effects in the TFD. At a given time n, a TFD $S_n[b',f]$ is estimated as

$$S_n[b',f] = W_n[b',f] \otimes \Phi[b',f] \tag{11}$$

where $W_n[b',f]$ is the Wigner–Ville distribution of $Y_{\mathrm{D}}[n,b']$ [21], estimated along b', $\Phi[b',f]$ is the elliptical exponential kernel used in [22] and [23], and $\otimes$ represents convolution on both time and frequency. An aggregate TFD, $S[b',f]$, is estimated by averaging $S_n[b',f]$ over n. $S_n[b',f]$ is down-sampled by a factor 2, and $V_{\mathrm{TFD}}[b] = S[b, f = 0.5]$. The detection statistic is defined as

$$Z_{\mathrm{TFD}}[b] = \frac{S[b, f = 0.5] - S_{\mathcal{N}}[b]}{\sigma_{\mathcal{N}}^{(\mathrm{S})}[b]} \tag{12}$$

where $S_{\mathcal{N}}[b]$ and $\sigma_{\mathcal{N}}^{(\mathrm{S})}[b]$ are defined as in (3). In this study, time and frequency resolutions (estimated as full width at half maximum of the kernel [21]) are 10 beats and 0.04 cpb, respectively.

B. EGM-TWA Detection: A Unified Statistical Approach

To decide whether EGM-TWA is present in an EGM, a test based on surrogate data is used [19]. Surrogate data for EGM-TWA test are generated by permuting randomly the order of the heart beats in $Y[n,b]$. The randomization destroys the alternating pattern of EGM-TWA while preserving the morphology of the T-waves, and a detection threshold is found which is related to the probability of erroneously detecting EGM-TWA merely due to random fluctuations. The procedure used in this study is described in Section III-C.

III. Comparative Simulation Study

This section describes the procedure to generate synthetic EGM with and without EGM-TWA from *in vivo* in human recordings, simulate the effect of different kinds of noise, and evaluate EGM-TWA detection performance.

TABLE I
Proportion of Positive, Bipolar and Negative T-Waves

Cycle Length [ms]	400	450	500	550
Pos./Bipolar/Neg. [%]	52/10/38	47/16/37	53/16/31	62/13/26

A. From Real Data to Simulated EGM

Multielectrode epicardial EGM were recorded from a patient undergoing cardiac surgery for coronary artery disease. Pacing was established from the epicardial left ventricle over a range of 4 cycle lengths ($T_{\mathrm{CL}} = 550, 500, 450, 400$ ms). Signals from $M = 120$ electrodes were selected and for each electrode a template representing the basic EGM, $x_i[n]$, $i = 1, \ldots, M$, was constructed by averaging over different heart beats. Depolarization times, τ_i, and the onset of the T-wave, J_i, were estimated for each template. To determine the polarity of the T-wave, each $x_i[n]$ was rescaled as $x_i[n] - x_i[n = J_i]$, and the ratio between the area under the positive part of the T-wave and the total area, α_i, was estimated. An EGM was considered positive, bipolar, or negative when $\alpha > 0.66$, $0.33 \leq \alpha \leq 0.66$, and $\alpha < 0.33$, respectively. The proportion of positive, bi-polar, and negative $x_i[n]$ is reported in Table I, while examples of $x_i[n]$ are shown in Fig. 1.

The procedure to generate EGM with the desired pattern of alternans from any electrode was 1) the amplitude of the T-wave, A_i^{T}, was estimated as the global maximum for positive template and global minimum for negative and bipolar template. 2) A template for EGM-TWA within each beat, $\Pi_i[n]$, was created as $\Pi_i[n] = 0$ for $n \leq J_i$ and $\Pi_i[n] = 1$ for $n > J_i$. 3) A beat-to-beat pattern of EGM-TWA was generated as

$$\mathcal{T}[b] = \begin{cases} 0.5(-1)^b + u & 32 < b \leq 96 \\ u & \text{otherwise} \end{cases} \tag{13}$$

where $b = 1, \ldots, B = 128$, and u is a random variable uniformly distributed between ± 0.125. A realization of $\mathcal{T}[b]$ is shown in Fig. 2. 4) EGM with added EGM-TWA was generated by modifying the templates:

$$X_i[n,b] = x_i[n] + V_0 A_i^{\mathrm{T}} \Pi_i[n] \mathcal{T}[b] \tag{14}$$

where V_0 indicates the relative magnitude of EGM-TWA with respect to the amplitude of the T-wave. 5) An EGM, $y_i^0[n]$, was finally generated by concatenating the B heart beats of $X_i[n,b]$ and low-pass filtering at 25 Hz. Summarizing, EGM recorded from 120 electrodes from the *in vivo* human heart were selected, and for each electrode a template $x_i[n]$ representing the basic heart beat was derived. EGM-TWA is present during 64 consecutive beats of the 128-beat-long test sequence, with an average magnitude V_0 times the magnitude of the T-wave, A_i^{T}. A random fluctuation in the magnitude of the T-waves, representing intrinsic variability in the action potential duration, is also introduced by adding u. An example of $X_i[n,b]$ with $V_0 = 5\%$ is shown in Fig. 1(d)–(f) (only $n \in [101, 300]$ is shown). Note that the filtering cancels any abrupt change in the morphology of the EGM.

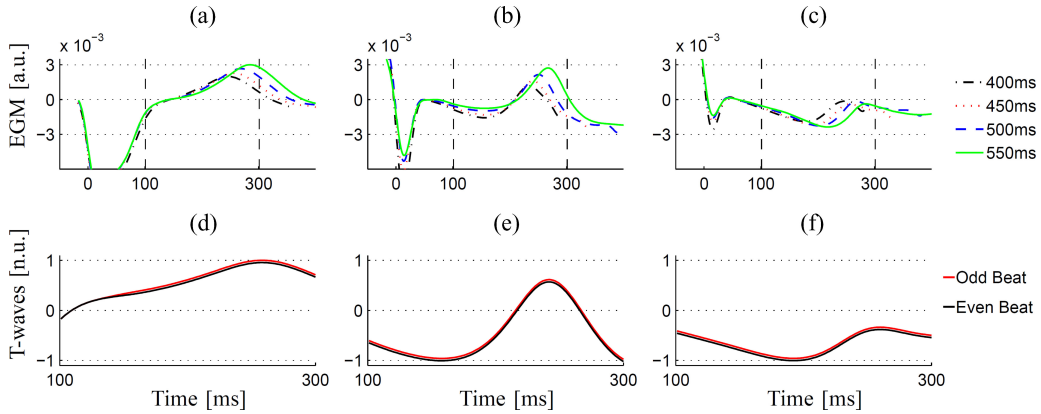

Fig. 1. (a)–(c): Examples of positive, bi-polar, and negative templates for EGM. Templates are estimated as described in the text. In the graphics, coordinates (x, y) are transformed so that the point $(0, 0) \equiv (\tau, J)$. Different line styles represent different cycle lengths. (d)–(e): Two consecutive T-waves (cycle length = 450 ms) in presence of EGM-TWA, before adding noise. T-waves are normalized. The magnitude of EGM-TWA is $V_0 = 5\%$ the amplitude of the T-wave A_i^{T}.

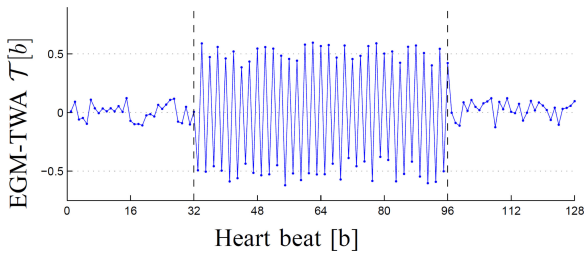

Fig. 2. Pattern of EGM-TWA $\mathcal{T}[b]$, representing the beat-to-beat fluctuations in the T-wave.

B. Simulating the Effect of Noise

1) Wide-Band Noise: Wide band disturbances, such as muscular noise, electrical interferences, or any other source of noise which can degrade the quality of the signal, should be taken into account. These kinds of disturbances are especially important for EGM which are often recorded in noisy conditions. The effect of electrical and muscular interferences was simulated by adding the Gaussian white noise to $y_i^0[n]$:

$$y_i[n] = y_i^0[n] + \xi_i[n]; \quad \text{with } \xi_i[n] \sim \mathcal{N}(0, A_i^{\mathrm{N}} A_i^{\mathrm{T}}) \qquad (15)$$

where $\xi_i[n]$ has zero mean and standard deviation equal to A_i^{N} times the T-wave amplitude. The Signal-to-noise ratio (SNR) is estimated as the ratio between powers of $y_i^0[n]$ and $\xi_i[n]$. Alternans to noise ratio (ANR) is defined as $(V_0/A_i^{\mathrm{N}})^2$.

2) Respiration: Respiration modulates the heart rate and the amplitude of the T-wave and, more recently, it has been shown to affect the action potential duration even at constant heart rates [24]. Thus, the effect of respiration on EGM-TWA estimates should be investigated. In this study, the heart rate is constant and the effect of respiration is simulated as an amplitude modulation:

$$y_i[n] = A_i^{\mathrm{R}}(1 + r^3[n]) y_i^0[n] + \xi_i[n] \qquad (16)$$

where $r[n]$ is a periodic signal with a cycle length that is a multiple of the pacing cycle length T_{CL}. $r[n]$ has a period $T_{\mathrm{CL}} n_{\mathrm{CL}}$ and is defined as

$$r[n] = \begin{cases} 2n/(T_{\mathrm{CL}} n_{\mathrm{CL}}) & 0 < n \le \frac{1}{2} T_{\mathrm{CL}} n_{\mathrm{CL}} \\ -4n/(T_{\mathrm{CL}} n_{\mathrm{CL}}) + 3 & \frac{1}{2} T_{\mathrm{CL}} n_{\mathrm{CL}} < n \le \frac{3}{4} T_{\mathrm{CL}} n_{\mathrm{CL}} \\ 0 & \frac{3}{4}(T_{\mathrm{CL}} n_{\mathrm{CL}}) < n \le T_{\mathrm{CL}} n_{\mathrm{CL}}. \end{cases}$$

That is, during each respiratory cycle, $r[n]$ increases linearly from 0 to 1 in half the respiratory period, decreases to zero in the following quarter period, and remains there for the rest of the cycle. In this study, we use $n_{\mathrm{CL}} = \{4, \ldots, 8\}$, and $A_i^{\mathrm{R}} = \{5, 10, 20\}\% \, A_i^{\mathrm{T}}$. White noise is also added.

3) Impulse Noise: Another kind of disturbance is represented by impulse noise, which includes ectopic beats, movement artifacts, loss of capture during stimulation, etc. Impulse noise is simulated by replacing N_{I} heart beats with a Hann function whose maximum is equal to A_i^{T}, i.e., $A_i^{\mathrm{T}} \sin^2(\pi n/(N/1))$. Three conditions were simulated using the model in (14), in which the number of beats $X_i[n, b]$ replaced by Hann functions was equal to $N_{\mathrm{I}} = \{3, 6, 12\}$. The position of these beats is chosen randomly. EGM are obtained adding noise as in (15).

C. Detection Scheme

For each condition described in the previous section, $M = 120$ EGM from different electrodes were generated. Among these 120 EGM, 60 were EGM-TWA positive, i.e., (13)–(14) were used, and 60 were EGM-TWA negative, i.e., $X_i[n, b] = x_i[n]$ in (14). The proportion of EGM with negative and nonnegative T-waves was approximately the same in both groups of signals. For each condition (i.e., level of noise, respiratory rate and amplitude, and number of impulse noise events), and each one of the 120 electrodes, 50 EGM were simulated using different realizations of intrinsic noise u, additive noise $\xi_i[n]$, and locating impulse noise events in different positions. EGM-TWA detection was then performed on each one of these 50 EGM using the same detection threshold, estimated as follows: 50 surrogate EGM were obtained by reshuffling the heart beats of each original EGM. For all methods except TFD, other 150 surrogate EGM were generated by simulating 150 EGM and reshuffling the heart

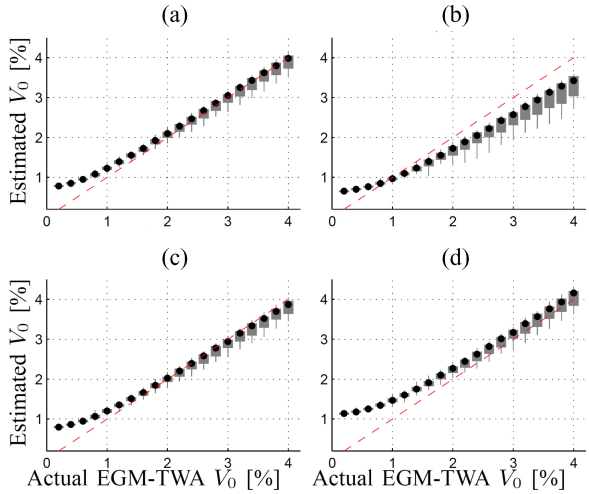

Fig. 3. Estimation of EGM-TWA magnitude. Each box represents the distribution of estimated EGM-TWA among channels. Standard deviation of added white noise was $A_i^{\mathrm{N}} = 0.1A_i^{\mathrm{T}}$. Dashed line represents line $x = y$. (a) SM. (b) MMA. (c) LLR. (d) TFD.

beats. Statistics $Z_{\mathrm{X}}^{\mathrm{S}}[b, r]$, with $X \in \{\mathrm{SM}, \mathrm{MMA}, \mathrm{LLR}, \mathrm{TFD}\}$ and $r = 1, \ldots, R$ were estimated for all R surrogate EGM ($R = 200$ for all methods except TFD, for which $R = 50$). A threshold $\gamma_{\mathrm{X}}^{\beta}$ was estimated as the β-percentile of the vector obtained by vectorization of $Z_{\mathrm{X}}^{\mathrm{S}}[b, r]$. EGM-TWA was detected whenever the statistic of an original EGM, $Z_{\mathrm{X}}[b]$, is higher than $\gamma_{\mathrm{X}}^{\beta}$ for at least $L_{\mathrm{Th}} = 12$ consecutive beats.

For each original EGM, sensitivity and specificity were estimated, and ROC curves produced. The area under the ROC curve A_{ROC} was used as a measure of detection performance.

IV. Results

A. Assessment of EGM-TWA Estimation

Fig. 3 shows that when signals were characterized by moderate to high SNR, there was a good agreement between actual and estimated EGM-TWA magnitude using all methods, even for low level of alternans. In the graphic, each boxplot represents the estimated magnitude of EGM-TWA for actual magnitude from $V_0 = 0.2\%$ to $V_0 = 4\%$ of A_i^{T}. Standard deviation of the white noise was $A_i^{\mathrm{N}} = 10\%$ of A_i^{T} (corresponding to a SNR of about 20 dB), which is 50 (and 2.5) times higher the lowest (the highest) magnitude of added EGM-TWA alternans. EGM-TWA was estimated as the mean value of $V_{\mathrm{X}}[b = 64]$, obtained averaging over 50 realizations, for a cycle length $T_{\mathrm{CL}} = 450$ ms. For $V_0 < 1\%$ all methods overestimated the actual level of EGM-TWA. For $V_0 > 1\%$, SM and LLR provided the most accurate estimates, while MMA underestimated EGM-TWA level.

B. EGM-TWA Detection and Wide-Band Noise

Fig. 4 shows that A_{ROC} is a function of $\mathrm{ANR} = (V_0/A_i^{\mathrm{N}})^2$. In this figure, A_{ROC} (mean and standard deviation) is plotted against ANR in a range going from 0.25%–4% (-26 to -14 dB): V_0 went from 0.5% to 5% (in steps of 0.5%), and A_i^{N} went from 2.5% to 100% of A_i^{T} (from about 32 to 0 dB). For constant ANR, approximately the same A_{ROC} was calculated, independently of V_0. The best results were obtained by LLR and SM: $A_{\mathrm{ROC}} > 0.9$ for ANR ≥ -20 dB, (ANR ≥ 0.01), and $A_{\mathrm{ROC}} > 0.8$ for ANR $= -22$ dB. The minimum magnitude of EGM-TWA which could be detected strictly depended on the quality of the recording. In particular, only EGM-TWA with a magnitude equal or higher than 10% the standard deviation of the noise (ANR ≥ -20 dB) was detected with high A_{ROC}. Fig. 5(a) shows the minimum V_0 which can be detected with $A_{\mathrm{ROC}} > 0.9$ for different level of noise. For a given V_0, a point represents the minimum SNR for which EGM-TWA was detected with $A_{\mathrm{ROC}} > 0.9$, while for a given SNR, a point represents the minimum V_0 associated with $A_{\mathrm{ROC}} > 0.9$. The best results were obtained by LLR and SM. Mean horizontal distance between SM or LLR and TFD or MMA was 1.98 dB. For example, EGM-TWA with magnitude $V_0 = 1\%$ was detected accurately by LLR and SM for SNR > 20.2 dB, and by MMA and TFD for SNR > 22.1 dB. Fig. 5(b)–(d) shows the accuracy, sensitivity, and specificity for the detection threshold corresponding to the 95th percentile ($\beta = 95$) of surrogate data distribution. For increasing ANR, the sensitivity decreased for all methods, being the decrease for MMA the most dramatic, while the specificity was almost constant. This figure shows the importance of selecting the appropriate detection threshold. The percentile which maximized the accuracy of the detection is shown in Table II.

TABLE II
β Corresponding to Maximum Accuracy (Mean $\pm$ SD)

	SM	MMA	LLR	TFD
ANR ≥ -20dB	95.1±1.8	78.8±6.1	98.1±1.1	99.6±0.5
ANR < -20dB	86.6±4.4	59.5±6.1	88.3±5.0	96.0±1.0

C. EGM-TWA Detection and Respiration

The effect of respiration is studied using the model described in (16). We investigated the influence of both the respiratory period, which was $n_{\mathrm{CL}} = \{4, \ldots, 8\}$ times longer than the cycle length, and the amplitude of the modulation, A_i^{R}, which went from 5% to 20% of A_i^{T}. In the results shown in Fig. 6, $V_0 = 1\%$ and $A_i^{\mathrm{N}} = 10\%$ (about 20 dB). Markers and bars represent mean and standard deviation of A_{ROC} over 50 realizations. A_{ROC} in absence of respiration ($A_i^{\mathrm{R}} = 0$) is reported for comparison on the left-hand column. Results show that respiration reduced the detection performance for any n_{CL} and T_{CL}. The degree of the reduction depended on the particular combination of n_{CL}, A_i^{R}, and T_{CL}. In general, the higher A_i^{R}, the lower A_{ROC}. The lowest A_{ROC} occurred for $n_{\mathrm{CL}} = 4$ and $n_{\mathrm{CL}} = 6$, for which, when $A_i^{\mathrm{R}} = 20\%$, A_{ROC} was as low as 0.5. Even for $A_i^{\mathrm{R}} = 5\%$, when $n_{\mathrm{CL}} = 4$, A_{ROC} decreased in comparison with A_{ROC} in absence of respiration 0.22, 0.16, 0.22, and 0.27 for SM, MMA, LLR, and TFD, respectively (averaging among T_{CL}). Importantly, for a heart rate of 109 bpm ($T_{\mathrm{CL}} = 550$ ms) and a respiratory rate of 18 breaths per minute ($n_{\mathrm{CL}} = 6$), A_{ROC} decreased about 0.075 for all methods [see panel (j)]. Among the 60 combinations taken into account (4 cycle lengths, 3 amplitude modulations, and 5 cycle lengths), MMA, SM, LLR, and TFD

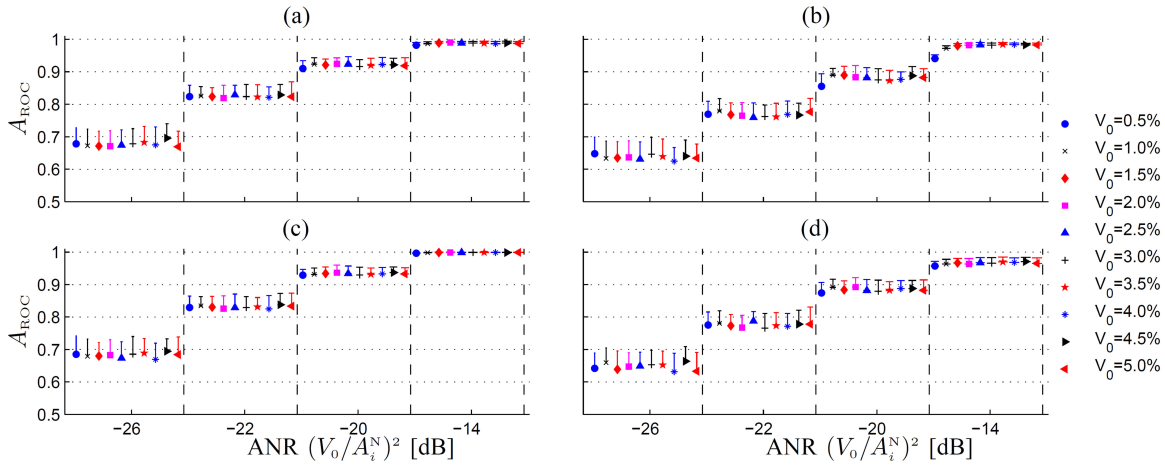

Fig. 4. EGM-TWA detection performance for different alternans to noise ratios (ANR). Dots and bars represents the mean and standard deviation of the area under the ROC curve, A_{ROC}. Magnitude of EGM-TWA, V_0, goes from 0.5% to 5%. In this example $T_{\mathrm{CL}} = 450$ ms. (a) SM. (b) MMA. (c) LLR. (d) TFD.

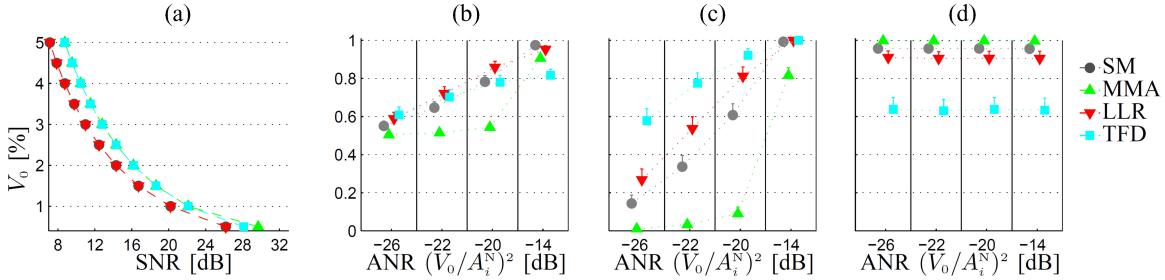

Fig. 5. (a) Minimum EGM-TWA magnitude, V_0, which can be detected with $A_{\mathrm{ROC}} > 0.9$ for different SNR. (b)–(d) Accuracy, sensitivity and specificity of EGM-TWA detection for different ANR. In these examples, $T_{\mathrm{CL}} = 450$ ms and V_0 goes from 0.5% to 5%.

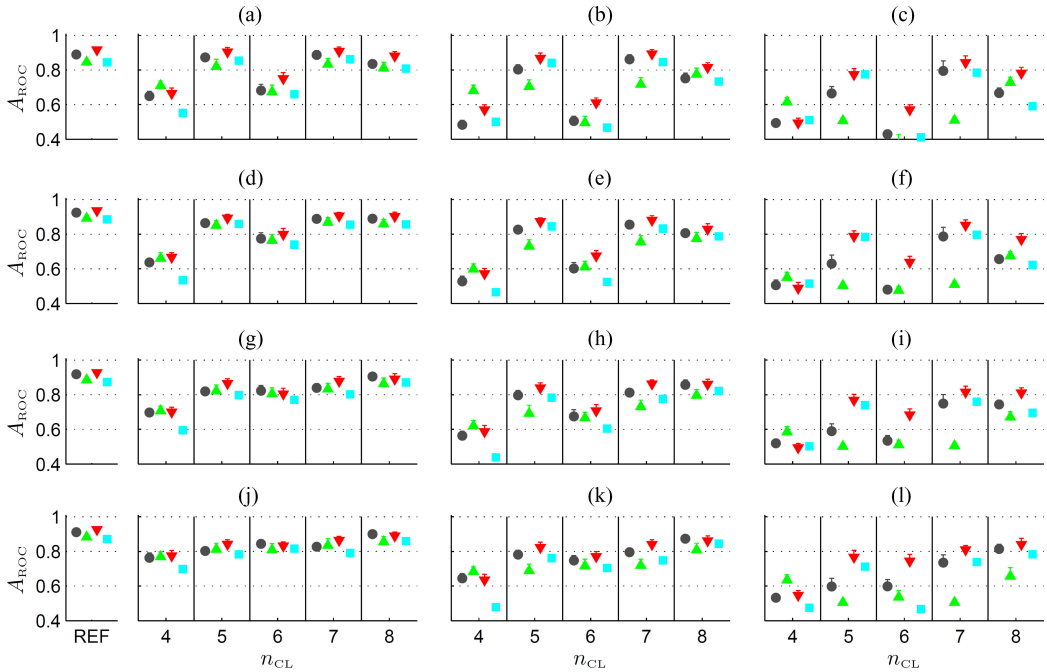

Fig. 6. Effect of respiration on EGM-TWA detection performance. EGM-TWA magnitude was $V_0 = 1\%$ of T-wave amplitude, standard deviation of white noise was $A_i^{\mathrm{N}} = 10\%$ of T-wave amplitude, SNR equal to about 20 dB. From left to right, colums represent the area under the ROC curve (A_{ROC}) for increasing respiratory modulation $A_i^{\mathrm{R}} = \{5\%, 10\%, 20\%\}$ of the T-wave amplitude. From top to bottom, lines represent results for different cycle lengths T_{CL}. Left hand column represents A_{ROC} in absence of respiration. Markers are as in Fig. 5: ○ (SM), △ (MMA), ▽ (LLR), □ (TFD) (a) $T_{\mathrm{CL}} = 400$ ms $A_i^{\mathrm{R}} = 5\%$. (b) $T_{\mathrm{CL}} = 400$ ms $A_i^{\mathrm{R}} = 10\%$. (c) $T_{\mathrm{CL}} = 400$ ms $A_i^{\mathrm{R}} = 20\%$. (d) $T_{\mathrm{CL}} = 450$ ms $A_i^{\mathrm{R}} = 5\%$. (e) $T_{\mathrm{CL}} = 450$ ms $A_i^{\mathrm{R}} = 10\%$. (f) $T_{\mathrm{CL}} = 450$ ms $A_i^{\mathrm{R}} = 20\%$. (g) $T_{\mathrm{CL}} = 500$ ms $A_i^{\mathrm{R}} = 5\%$. (h) $T_{\mathrm{CL}} = 500$ ms $A_i^{\mathrm{R}} = 10\%$. (i) $T_{\mathrm{CL}} = 500$ ms $A_i^{\mathrm{R}} = 20\%$. (j) $T_{\mathrm{CL}} = 550$ ms $A_i^{\mathrm{R}} = 5\%$. (k) $T_{\mathrm{CL}} = 550$ ms $A_i^{\mathrm{R}} = 10\%$. (l) $T_{\mathrm{CL}} = 550$ ms $A_i^{\mathrm{R}} = 20\%$.

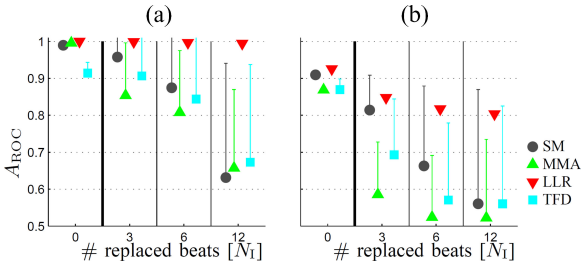

Fig. 7. Effect of impulse noise on EGM-TWA detection performance. Markers and bars represent mean and standard deviation of A_{ROC} averaging among realizations and cycle lengths. (a) $V_0 = 1\%$, $A_i^{\mathrm{N}} = 10\%\, A_i^{\mathrm{T}}$. (b) $V_0 = 5\%$, $A_i^{\mathrm{N}} = 25\%\, A_i^{\mathrm{T}}$.

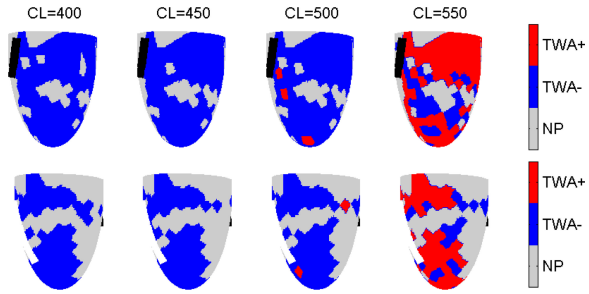

Fig. 8. EGM-TWA mapping: upper and lower graphics represent the left and right ventricles, respectively. The left anterior descending artery is plotted in black. EGM-TWA positive and negative sites are in red and blue, respectively. Regions from where EGMs were either too noisy or not recorded are in gray.

were associated to the highest A_{ROC} in 5, 10, 44, and 1 cases, respectively.

D. EGM-TWA Detection and Impulse Noise

Impulse noise is used to simulate the effect of an event which introduces one or more artifacts into the analyzed sequences of T-waves. Fig. 7 shows that impulse noise had a dramatic effect on the detection performance of all methods, but LLR. In panel (b), it is shown that for $V_0 = 1\%$ and $A_i^{\mathrm{N}} = 10\%$, LLR had $A_{\mathrm{ROC}} > 0.80$ even when 12 heart beats over 128 were replaced by artifactual ones, while all the other methods had $A_{\mathrm{ROC}} < 0.60$. Similar results are shown in panel (b), for $V_0 = 5\%$ and $A_i^{\mathrm{N}} = 10\%$. Moreover, the standard deviation of A_{ROC} for LLR was much lower than for any other method. This suggests that the detection performance of LLR was not affected by the position of impulse noise events and cycle lengths.

E. EGM-TWA Detection, T-Wave Localization, and Morphology

The mean and standard deviation of the estimation error of depolarization times, $\tau_i[b] - \hat{\tau}_i[b]$, used to localize the T-waves, was a linear function of A_i^{N}: mean error was equal to $0.775\, A_i^{\mathrm{N}} + 1.47$ ($R^2 = 0.995$) and the standard deviation was $6.69 A_i^{\mathrm{N}} + 2.87$ ($R^2 = 0.996$). For example, for SNR between 20 and 30 dB the estimation error was equal to 1.53 ± 3.33 ms. The error in the localization of the T-wave caused a minor reduction of A_{ROC}: grouping together all conditions (different level of noise, number of impulse noise events, respiratory rate, and amplitude) average reduction of A_{ROC} with respect to the case in which actual $\tau_i[b]$ were used to localize the T-wave was lower than 0.012.

When the effect of white noise, respiration, and impulse noise are considered all together, no differences were observed between A_{ROC} for negative and nonnegative T-waves.

F. In Vivo Epicardial Mapping of the Intact Human Heart

The EGMs used to generate the templates and the synthetic signals were analyzed and results are shown in Fig. 8. For each cycle length, a sequence of about 35 beats was recorded and analyzed with the LLR method. The length of the window used for the calculation, L, was set equal to the length of each EGM series, and the detection threshold corresponded to the 95th percentile of a distribution of 200 surrogate EGM. Upper and lower panles represent the left and right ventricles, respectively. Sites where EGM-TWA was statistically significant are represented in red. These results demonstrate the capability of LLR for detecting EGM-TWA in EGM recorded *in vivo* in humans, and show that local EGM-TWA is characterized by heterogeneous spatio-temporal distribution. In this example, EGM-TWA was more apparent at a cycle length of 550 ms than at shorter cycle lengths.

V. Discussion

In this paper, we compared the detection performance of four methods for EGM-TWA quantification/detection in synthetic unipolar EGM based on *in vivo* in human recordings. We considered short EGM recordings, $N = 128$ beats, at fixed cycle lengths to reproduce the typical conditions in which electrophysiological studies are usually conducted. The stabilization of the heart rate by means of external stimulation at a fixed cycle length offers the opportunity of studying repolarization dynamics independently of heart rate variability, which is considered as a source of noise. Methodologies for EGM-TWA estimation/detection should be characterized by a good temporal resolution, since it has been shown that EGM-TWA can appear in short sequences of only few beats [10]–[12]. Accordingly, in this study, EGM-TWA was added in only 64 heart beats.

The main results of the study were: 1) EGM-TWA can be detected accurately only when its magnitude is equal or higher than 10% the standard deviation of the noise (ANR ≥ -20 dB). This implies that knowing the noise level, it is possible to estimate the minimum level below which EGM-TWA measures should be disregarded as false alarms. 2) Respiration can be critical for EGM-TWA analysis, even at usual respiratory rates. 3) Impulse noise strongly reduces the accuracy of all methods, except LLR. 4) The polarity of the T-wave does not affect the detection rate. 5) If depolarization time is used as a fiducial point, the localization of the T-wave is not critical for the accuracy of EGM-TWA detection.

A. Unified Detection Scheme

In this study, we used a nonparametric decision scheme based on surrogate data [19]. The main advantage of this scheme is that it is model-free, and therefore it does not depend on how

well the model explains data and noise. Moreover, it can be used with any statistic and is particularly useful for those methodologies, such as MMA and TFD, which do not include a specific decision scheme. Furthermore, using surrogate data, the number of false positive detection, which determines the specificity of the detection scheme, is independent of the quality of the signal. This is apparent in Fig. 5(d). The idea of using the original data to estimate a discrimination threshold was already proposed in [13], where measures of ECG-TWA obtained through MMA where compared with measures of ECG-TWA obtained in series of even and odd beats separately. However, the use of even and odd beats to estimate a discrimination threshold may be inappropriate when the respiratory period is a multiple of the R-R interval, since respiration can introduce alternations in every-other-beat in odd and even series. A surrogate based test for ECG-TWA detection was proposed and evaluated in [19], while a parametric test has been recently proposed to detect repolarization alternans in optical mapping data [25].

B. Methodological Comparison

The accuracy of the detection of EGM-TWA was assessed in presence of white noise, periodical noise, and impulse noise, for both positive and negative T-waves. LLR was as accurate as SM when white noise was added, and performed better than any other methods when respiration and impulse noise were taken into account. In particular, unlike other methodologies, LLR was robust against impulse noise. This is an important feature, since EGM are often corrupted by artifacts, such as ectopic beats, loss of contact between the electrode and the myocardium, loss of capture during stimulation, etc. These kinds of artifacts cannot be easily removed. Thus, a methodology which performs accurately even in presence of these artifacts is suitable. The reason why LLR is more robust than the other methods may be that $Z_{\mathrm{LLR}}[b]$ is estimated using only terms which do not exceed the maximum likelihood estimation of the alternans wave, $v[n,k]$, which in turn is based on a robust estimator, i.e., the median.

The use of time-frequency analysis instead of classical spectral analysis did not result in any improvement. This may be due to the fact that a better time-frequency resolution is achieved at the detriment of robustness against noise and artifacts. A methodology which combines sharp time-frequency localization with reduction of the variance of the estimation, such as the multitaper reassignment, recently proposed for EGM-TWA detection [26], or adaptive time-frequency analysis [27], may be beneficial. However, time-frequency analysis requires much more computational load than classical spectral analysis.

The comparison performed in this study is based on the detection performance in rather specific situations. It is worth noting that SM and TFD provide more information than the amplitude of alternans, such as the magnitude of respiratory-related oscillations, and phase relationship. In this study, we focused on the most used methods, SM, MMA, and LLR, and we assessed a novel one, TFD, but other techniques [11] can be studied in future work.

C. EGM-TWA and Respiration

Although the effect of respiration has been already recognized as potentially detrimental for alternans detection [17], to the extent of our knowledge, this effect was never quantified before. Respiration modulates the amplitude and the duration of the T-wave, thus introducing oscillations which can overlap or get confused with EGM-TWA. In theory, this can happen only when the respiratory rate is $2n$ times higher than the heart rate, since in this case a harmonic of the respiration can fall at frequency 0.5 cpb. We showed that the accuracy of the detection can decrease even for respiratory rate six times lower than the heart rate, i.e., at 0.42, 0.37, 0.33, and 0.30 Hz for cycle lengths equal to 400, 450, 500, and 550 ms, respectively, which are usual respiratory rates. Moreover, the respiratory modulation of the EGM also reduced the accuracy of the detection when the respiratory rate was not $2n$ times higher the heart rate, as for $n_{\mathrm{CL}} = 5$ and 7. Several aspects should be investigated further. First, in this study, we have simulated the effect that respiration exerts on repolarization at a constant heart rate, i.e., independently of respiratory sinus arrhythmia [24]. When EGM are recorded at sinus rhythm, the duration of the T-wave may also change with respiration. This may slightly increase the effect that respiration exerts on EGM-TWA analysis and should be studied. Second, the effect of respiration also depends on the profile of the modulation, which determines the magnitude of its harmonics. In this study, inspiration was longer than expiration. More symmetric modulations produce less prominent harmonics, thus likely reducing the effect of respiration on EGM-TWA detection. Third, it is unlikely that respiratory frequency is constantly locked to the heart rate for a long period of time, and the effect of nonstationary respiratory rate may also deserve attention in future studies.

D. Implications and Future Lines

In the application to real signals, we illustrate that repolarization alternans is a complex phenomenon with heterogeneous spatio-temporal distribution, which should be studied and related to noninvasive markers of EGM-TWA. In this human case study, EGM-TWA was significant at paced cycle lengths of 550 and 600 ms (not shown) but was less apparent at shorter cycle lengths. Ongoing work will confirm whether this trend is consistent in other subjects; if that is the case, the finding would imply that *in vivo* local EGM-TWA is inhibited in paced heart rates higher than 110 bpm, and it would have an impact in the understanding of the aetiology of repolarization alternans. The precise relationship between EGM-TWA and ECG-TWA is still unclear, and it may be possible that ECG-TWA and EGM-TWA do not present a parallel rate dependence.

Although this study focused on EGMs recorded on the myocardium, there are strong similarities with alternans analysis in body-surface potentials: both types of signals have similar morphology, the considered sources of noise are expected to produce similar effects, and a correlation exists between repolarization alternans in EGMs recorded on the myocardium and on the body surface [13], [28]. These similarities suggest that the results presented here may be more widely applicable and

that investigation of that broader applicability would be justified. Respiration can be an issue for EGM-TWA detection and should be monitored during EGM-TWA tests. More work is required to evaluate the effect of respiration in real data, and design algorithms which reduce its effect. Impulse noise has been shown to have a dramatic effect on the detection performance on common methods for EGM-TWA detection. Given that this is a common source of noise, one should either use robust techniques, such as LLR, or find a strategy to replace impulse noise events [18]. Table II and Fig. 5 show that, although noise estimates are incorporated in the statistics $Z[b]$, the threshold which maximizes the accuracy of the detection depends on ANR. A strategy to make the accuracy of the detection independent of the noise level would be highly beneficial.

VI. Conclusion

In this study, we assessed and compared four methodologies for EGM-TWA estimation/detection in relation to the quality of the recordings, the presence of artifacts, and the interference of respiration. We showed that EGM-TWA can be detected accurately if the alternans to noise ratio is higher than 0.01. Respiration was shown to be critical for EGM-TWA detection even at usual respiratory rates, the jitter in the localization of the T-wave only slightly reduced the accuracy of the detection, and the morphology and polarity of the T-wave did not affect EGM-TWA analysis. Impulse noise dramatically reduced the detection performance of all methods except LLR, which was also more robust against the effect of respiration. Finally, we characterized the complex spatio-temporal distribution of epicardial EGM-TWA in a patient undergoing cardiac surgery.

References

[1] R. Verrier, T. Klingenheben, M. Malik, N. El-Sherif, D. Exner, S. Hohnloser, T. Ikeda, J. P. Martínez, S. Narayan, T. Nieminen, and D. Rosenbaum, "Microvolt T-wave alternans: Physiological basis, methods of measurement, and clinical utilityconsensus guideline by international society for holter and noninvasive electrocardiology," *J. Amer. College Cardiol.*, vol. 58, no. 13, pp. 1309–1324, 2011.

[2] V. Monasterio, P. Laguna, I. Cygankiewicz, R. Vázquez, A. Bayés-Genís, A. Bayés de Luna, and J. P. Martínez, "Average T-wave alternans activity in ambulatory ECG records predicts sudden cardiac death in patients with chronic heart failure," *Heart Rhythm*, vol. 9, no. 3, pp. 383–389, 2012.

[3] L. D. Wilson and D. S. Rosenbaum, "Mechanisms of arrythmogenic cardiac alternans." *Europace*, vol. 9, Suppl 6, pp. vi77–vi82, 2007.

[4] J. M. Pastore, S. D. Girouard, K. R. Laurita, F. G. Akar, and D. S. Rosenbaum, "Mechanism linking T-wave alternans to the genesis of cardiac fibrillation.," *Circulation*, vol. 99, no. 10, pp. 1385–1394, 1999.

[5] J. P. Martínez and S. Olmos, "Methodological principles of T-wave alternans analysis: A unified framework," *IEEE Trans. Biomed. Eng.*, vol. 52, no. 4, pp. 599–613, Apr. 2005.

[6] K. Laurita and D. Rosenbaum, "Cellular mechanisms of arrhythmogenic cardiac alternans," *Progr. Biophys. Molecul. Biol.*, vol. 97, no. 2–3, pp. 332–347, 2008.

[7] M. Potse, A. Vinet, T. Opthof, and R. Coronel, "Validation of a simple model for the morphology of the T wave in unipolar electrograms," *Amer. J. Physiol. Heart Circ. Physiol.*, vol. 297, no. 2, pp. H792–H801, 2009.

[8] D. Gordon, A. Kadish, D. Koolish, T. Taneja, J. Ulphani, J. Goldberger, and J. Ng, "High-resolution electrical mapping of depolarization and repolarization alternans in an ischemic dog model," *Amer. J. Physiol. Heart Circ. Physiol.*, vol. 298, no. 2, pp. H352–H359, 2010.

[9] V. Chauhan, E. Downar, K. Nanthakumar, J. Parker, H. Ross, W. Chan, and P. Picton, "Increased ventricular repolarization heterogeneity in patients with ventricular arrhythmia vulnerability and cardiomyopathy: A human *in vivo* study," *Amer. J. Physiol. Heart Circ. Physiol.*, vol. 290, no. 1, pp. H79–H86, 2006.

[10] E. Weiss, F. Merchant, A. D'Avila, L. Foley, V. Reddy, J. Singh, T. Mela, J. Ruskin, and A. Armoundas, "A novel lead configuration for optimal spatio-temporal detection of intracardiac repolarization alternans," *Circ. Arrhythm Electrophysiol.*, vol. 4, no. 3, pp. 407–417, 2011.

[11] C. Swerdlow, X. Zhou, O. Voroshilovsky, A. Abeyratne, and J. Gillberg, "High amplitude T-wave alternans precedes spontaneous ventricular tachycardia or fibrillation in ICD electrograms," *Heart Rhythm*, vol. 5, no. 5, pp. 670–676, 2008.

[12] C. Swerdlow, T. Chow, M. Das, A. Gillis, X. Zhou, A. Abeyratne, and R. Ghanem, "Intracardiac electrogram T-wave alternans/variability increases before spontaneous ventricular tachyarrhythmias in implantable cardioverter- defibrillator patients: A prospective, multi-center study," *Circulation*, vol. 123, no. 10, pp. 1052–1060, 2011.

[13] R. Selvaraj, P. Picton, K. Nanthakumar, S. Mak, and V. Chauhan, "Endocardial and epicardial repolarization alternans in human cardiomyopathy. evidence for spatiotemporal heterogeneity and correlation with body surface T-wave alternans," *J. Amer. College Cardiol.*, vol. 49, no. 3, pp. 338–346, 2007.

[14] O. Paz, X. Zhou, J. Gillberg, H.-J. Tseng, E. Gang, and C. Swerdlow, "Detection of T-wave alternans using an implantable cardioverter-defibrillator," *Heart Rhythm*, vol. 3, no. 7, pp. 791–797, 2006.

[15] D. Christini, K. Stein, S. Hao, S. Markowitz, S. Mittal, D. Slotwiner, S. Iwai, M. Das, and B. Lerman, "Endocardial detection of repolarization alternans.," *IEEE Trans. Biomed. Eng.*, vol. 50, no. 7, pp. 855–862, Jul. 2003.

[16] B. Nearing and R. Verrier, "Progressive increases in complexity of T-wave oscillations herald ischemia-induced ventricular fibrillation," *Circulat. Res.*, vol. 91, no. 8, pp. 727–732, 2002.

[17] D. Bloomfield, S. Hohnloser, and R. Cohen, "Interpretation and classification of microvolt T-wave alternans tests," *J. Cardiovasc. Electrophysiol.*, vol. 13, no. 5, pp. 502–512, 2002.

[18] A. A. Armoundas, T. Mela, and F. M. Merchant, "On the estimation of T-wave alternans using the spectral fast fourier transform method," *Heart Rhythm*, vol. 9, no. 3, pp. 449–456, 2012.

[19] S. Nemati, O. Abdala, V. Monasterio, S. Yim-Yeh, A. Malhotra, and G. D. Clifford, "A nonparametric surrogate-based test of significance for T-wave alternans detection.," *IEEE Trans. Biomed. Eng.*, vol. 58, no. 5, pp. 1356–1364, May 2011.

[20] J. P. Martínez, S. Olmos, G. Wagner, and P. Laguna, "Characterization of repolarization alternans during ischemia: Time-course and spatial analysis," *IEEE Trans. Biomed. Eng.*, vol. 53, no. 4, pp. 701–711, Apr. 2006.

[21] M. Orini, R. Bailon, L. T. Mainardi, P. Laguna, and P. Flandrin, "Characterization of dynamic interactions between cardiovascular signals by time-frequency coherence," *IEEE Trans. Biomed. Eng.*, vol. 59, no. 3, pp. 663–673, Mar. 2012.

[22] M. Orini, P. Laguna, L. T. Mainardi, and R. Bailón, "Assessment of the dynamic interactions between heart rate and arterial pressure by the cross time-frequency analysis.," *Physiol. Meas.*, vol. 33, no. 3, pp. 315–331, 2012.

[23] M. Orini, R. Bailón, P. Laguna, L. T. Mainardi, and R. Barbieri, "A multivariate time-frequency method to characterize the influence of respiration over heart period and arterial pressure," *EURASIP J. Adv. Signal Process.*, vol. 2012, no. 1, pp. 1–17, 2012.

[24] B. Hanson, J. Gill, D. Western, M. P. Gilbey, J. Bostock, M. R. Boyett, H. Zhang, R. Coronel, and P. Taggart, "Cyclical modulation of human ventricular repolarization by respiration," *Front Physiol.*, vol. 3, art. no. 379, pp. 1–12, 2012.

[25] S. Iravanian, U. Kanu, and D. Christini, "A class of monte-carlo-based statistical algorithms for efficient detection of repolarization alternans," *IEEE Trans. Biomed. Eng.*, vol. 59, no. 7, pp. 1882–1891, Jul. 2012.

[26] M. Orini, B. Hanson, P. Taggart, and P. D. Lambiase, "Detection of transient, regional cardiac repolarization alternans by time-frequency analysis of synthetic electrograms," in *Proc. Int. Conf. IEEE Eng. Med. Biol. Society*, 2013, pp. 3773–3776.

[27] B. Ghoraani, S. Krishnan, R. Selvaraj, and V. Chauhan, "T wave alternans evaluation using adaptive time-frequency signal analysis and non-negative matrix factorization," *Med. Eng. Phys.*, vol. 33, no. 6, pp. 700–711, 2011.

[28] A. A. Armoundas, E. H. Weiss, O. Sayadi, S. Laferriere, N. Sajja, T. Mela, J. P. Singh, C. D. Barrett, E. K Heist, and F. M. Merchant, "A novel pacing method to suppress repolarization alternans in vivo: implications for arrhythmia prevention," *Heart Rhythm*, vol. 10, no. 4, pp. 564–572, Apr. 2013.

Authors' photographs and biographies not available at the time of publication.